MANUSCRIPT FILE

Constitutive activity of ionotropic glutamate receptors via a hydrophobic plug in the ligand-binding domain

Sandra Seljeset[1], Oksana Sintsova[1], Yuhong Wang[1], Hassan Y. Harb[2], Timothy Lynagh[1*]

[1] Michael Sars Centre, University of Bergen, 5008 Bergen, Norway

[2] Concept Life Sciences Limited, Frith Knoll Road, Chapel-en-le-Frith, High Peak, SK23 0PG, United Kingdom

*Correspondence, tim.lynagh@uib.no

SUMMARY

Neurotransmitter ligands electrically excite neurons by activating ionotropic glutamate receptor (iGluR) ion channels. Knowledge of the iGluR amino acid residues that dominate ligand-induced activation would enable the prediction of function from sequence. We therefore explored determinants of activity in rat NMDA-type iGluRs (NMDA receptors), complex heteromeric iGluRs comprising two glycine-binding GluN1 and two glutamate-binding GluN2 subunits, using amino acid sequence analysis, mutagenesis, and electrophysiology. We find that a broadly conserved aspartate residue controls both ligand potency and channel activity, to the extent that certain substitutions at this position bypass the need for ligand-binding in GluN1 subunits, generating NMDA receptors activated solely by glutamate. Furthermore, we identify a homomeric iGluR from the placozoan *Trichoplax adhaerens* that has utilized this crucial residue to evolve into a leak channel that is inhibited by neurotransmitter binding, pointing to a dominant role of this residue throughout the iGluR superfamily.

KEYWORDS

binding site, glutamate, iGluR, ion channels, LBD, ligand-gated ion channels, neurotransmitter receptors, NMDA receptor, Placozoa, spontaneous activity

INTRODUCTION

Neurons rapidly signal to each other via chemical synapses, where neurotransmitter released by one cell diffuses across a narrow synaptic cleft and binds to ligand-gated ion channels (LGICs), or "ionotropic receptors", on the postsynaptic cell membrane (1, 2). LGICs are membrane proteins with extracellular ligand-binding domains (LBDs) and a membrane-spanning channel domain. Ligand-binding in the LBD triggers conformational changes that open (i.e. "gate") the channel within milliseconds, mediating rapid ion flux across the cell membrane. This depolarizes the postsynaptic neuron in the case of excitatory, Na^+-permeable channels, typified by ionotropic glutamate receptors (iGluRs), the major excitatory receptor in the mammalian brain (3, 4).

iGluRs are tetramers, formed by the assembly of four homologous subunits around a central channel pore, with each subunit contributing its own extracellular LBD (4). The iGluR superfamily is broad, but most members bind the transmitters glutamate or glycine, and the superfamily can be divided into several families based on functional differences and phylogenetic relationships (5). Mammalian synapses typically contain iGluRs from two families: α-amino-3-hydroxy-5-methyl-4-isoxazolepropionate-sensitive iGluRs (AMPA receptors); and N-methyl-D-aspartate-sensitive iGluRs (NMDA receptors). Like primitive iGluRs in bacteria and early-branching animals (6, 7), AMPA receptors are homo-tetramers – or hetero-tetramers with a mix of closely related GluA1-GluA4 subunits – that rapidly activate and deactivate in response to glutamate and conduct mostly Na^+ and K^+ *in vivo* (8). In contrast, NMDA receptors are obligate hetero-tetramers, comprising two glycine- and D-serine-binding GluN1 subunits and two glutamate-binding GluN2 subunits, thus requiring two different ligands for channel opening (9). NMDA receptors are important "coincidence detectors" as they carry long-lasting Na^+ and Ca^{2+} currents *in vivo* only after channel block by Mg^{2+} ions is relieved by AMPA receptor depolarization (10).

Channel gating requires ligand binding in the clamshell-shaped LBD, during which the lower lobe of the clamshell moves upward, away from the cell membrane. This opens the channel by pulling on the channel-lining α-helices via short peptide segments that link the LBD to the channel (11-13). LBD clamshell closure is a loosely conserved feature of glutamate-gated homo-tetramers, glycine-gated homo-tetramers, and glutamate and glycine-binding hetero-tetramers alike, as inferred by X-ray crystallographic structures of diverse iGluRs (6, 13, 14). However, several aspects of LBD activity deserve investigation. From a biophysical perspective where we seek to understand channel gating mechanisms, the contributions of four distinct LBDs to the gating of a shared, central channel remains unclear (15-17), and structural studies suggest that clamshell closure may not drive channel gating the same way in different iGluR families (18, 19). And from a biological and pharmacological perspective, predicting iGluR function from amino acid sequence remains difficult: despite high-resolution structural data, we don't entirely understand which LBD residues dominate ligand recognition and channel activity.

We have therefore investigated the role of one particular amino acid residue in iGluR activation. We focused on it because of its broad conservation as either a glutamate or aspartate residue in diverse iGluRs, its position in the middle of the LBD clamshell, and its previous implication in both ligand recognition and LBD conformational change. We began our study utilizing the glycine-binding GluN1 subunit of hetero-tetrameric NMDA receptors, where the residue in question is an aspartate, D732. X-ray crystallography studies have shown that the GluN1-D732 side chain orients away from the ligand-binding site in inactive receptor states but toward glycine in active receptor states (13, 20), and a mutagenesis study showed that even the relatively subtle D732E substitution drastically reduces the potency of glycine in activating GluN1 subunits (21). We explored the role of this residue in NMDA receptor activity and also in a distantly related homomeric iGluR, using mutagenesis, electrophysiology, and amino acid sequence analysis of diverse iGluRs. This uncovered a remarkably dominant contribution of this position to both ligand recognition and channel activity, not only in heteromeric NMDA receptors but also in distantly related homomeric iGluRs.

RESULTS

GluN1 D732L and -F substitutions yield NMDA receptors activated solely by glutamate

We first investigated the contribution of D732 to glycine-induced activation of GluN1 subunits by replacing it with amino acid residues of varying physico-chemical properties (Fig. 1A). We then measured currents through GluN1-mutant/GluN2A-wildtype receptors heterologously expressed in *Xenopus laevis* oocytes, in response to increasing glycine concentrations in the presence of 100 µM glutamate. Compared to wildtype (WT) channels, glycine potency was decreased 1,000-10,000-fold in channels with small side chains (D732A, D732S), with a longer carboxylate side chain (D732E), or with an isosteric but amide side chain (D732N) at the GluN1-D732 position (Fig. 1B), consistent with previous work on GluN1/GluN2B receptors (21). We also observed large decreases in glycine potency with β-branched hydrophobic D732V and D732I substitutions (Fig. 1A,B). Longer hydrophobic substitutions, however, had very different effects. At GluN1-D732L- and GluN1-D732F-containing receptors, we saw no glycine concentration-dependence of ligand-gated currents, with large currents already activated by 100 nM glycine/100 µM glutamate (Fig. 1B).

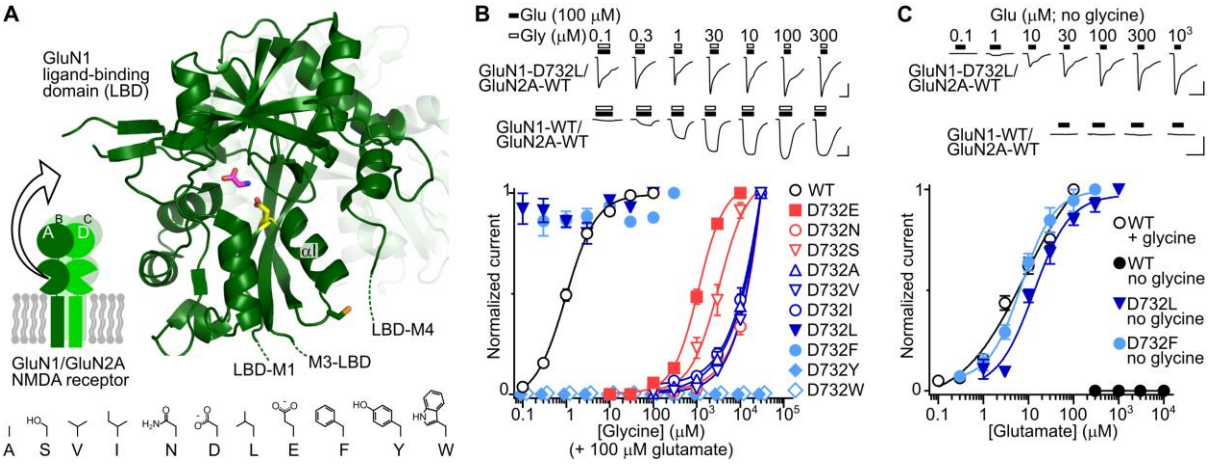

Figure 1. Certain hydrophobic side chains at the GluN1 732 position yield NMDA receptors activated solely by glutamate.
(A) *Mid-left*, cartoon hetero-tetrameric NMDA receptor showing GluN1 subunits (dark green), GluN2A subunits (light green), and surrounding cell membrane (grey). Note that GluN1 subunits occupy positions "A" and "C" in the tetramer when counted clockwise from above (22). *Main*, Bound glycine (magenta) and GluN1 D732 side chain (yellow) in previously published X-ray structure of NMDA receptor ligand-binding domain (PDB 4NF8). αI helix labelled and following C744 side chain shown. Dashed lines indicate approximate position of LBD-channel domain linkers. *Bottom*, amino acid side chain 2D structures.
(B) *Upper*, example glycine+glutamate-gated currents in *Xenopus laevis* oocytes expressing indicated GluN1/GluN2A receptors. Scale bars: x, 5 s; y, 1 µA. *Lower*, glycine concentration-current response relationships (data points: mean ± SEM, n = 6-7) for GluN1/GluN2A receptors carrying indicated GluN1 subunits.
(C) *Upper*, example glutamate-gated currents in the absence of glycine in oocytes expressing indicated GluN1/GluN2A receptors. Scale bars: x, 5 s; y, 1 µA. *Lower*, corresponding glutamate concentration-current response relationships (data points: mean ± SEM, n = 6-7).

Reasoning that this effect may derive from solely glutamate-gated currents in GluN1-D732L- and GluN1-D732F-containing receptors, we tested responses of these receptors to increasing concentrations of glutamate in the absence of glycine. Indeed, glutamate alone elicited concentration-dependent currents in GluN1-D732L/GluN2A-WT and GluN1-D732F/GluN2A-WT receptors (Fig. 1C), with a concentration-response relationship (glutamate EC_{50} 12.8 ± 2.0 µM and 7.1 ± 1.4 µM, respectively, both n = 6) that was very similar to that of glutamate at WT receptors in the presence of 100 µM glycine (glutamate EC_{50} 4.8 ± 0.5, n = 11, Fig. 1C). Tyrosine and tryptophan substitution in the same position did not induce the same effect, as we observed no glutamate- or glycine and glutamate-gated currents at oocytes injected with GluN1-D732Y or GluN1-D732W together with GluN2A-WT RNAs (Fig. 1B). These data show that essentially all substitutions at the GluN1-732 position decrease glycine potency, but leucine and phenylalanine substitutions also remove the requirement for glycine

co-agonism in GluN1/GluN2A NMDA receptors. This leads to single-mutant NMDA receptors that are activated solely by glutamate.

GluN1 D732L and D732F LBDs are constitutively active

Solely glutamate-gated currents at GluN1-D732L and D732F-containing receptors could be due to the L and F side chains conferring glutamate sensitivity on GluN1 LBDs, such that glutamate now binds to GluN1 and GluN2A subunits to activate the mutant receptors. Alternatively, the L and F side chains might induce an active GluN1 LBD conformation in the absence of ligand, such that glutamate activates the mutant receptors by only binding to GluN2A subunits, reflected in previous studies that locked GluN1 LBDs in an active state via introduced disulfide bonds (23, 24). To distinguish between these possibilities, we measured glutamate-gated currents in receptors comprising GluN1 double-mutant R523K/D732L and GluN2A-WT subunits. R523 is a highly conserved arginine residue in the LBD of diverse iGluRs, and in GluN1 and GluN2A subunits its guanidino side chain binds the α-carboxylate of glycine and glutamate, respectively, and its mutation to lysine greatly decreases agonist potency (25, 26). Receptors containing GluN1-R523K/D732L were potently activated by glutamate in the absence of glycine much like those containing GluN1-D732L (Fig. 2A, GluN1-R523K/D732L EC_{50} 3.5 ± 1.7 µM, n = 3), whereas receptors containing single-mutant GluN1-R523K were not activated by glycine and glutamate below 3 mM (n = 5, Fig. 2A). This suggests that glutamate activates GluN1-D732L-containing receptors by binding strictly to GluN2A-WT subunits, and D732L and D732F substitutions render GluN1 subunits constitutively active in a manner similar to glycine-binding. We picture the leucine and phenylalanine side chains as "hydrophobic plugs" in the GluN1 LBD that activate the subunit in the absence of glycine.

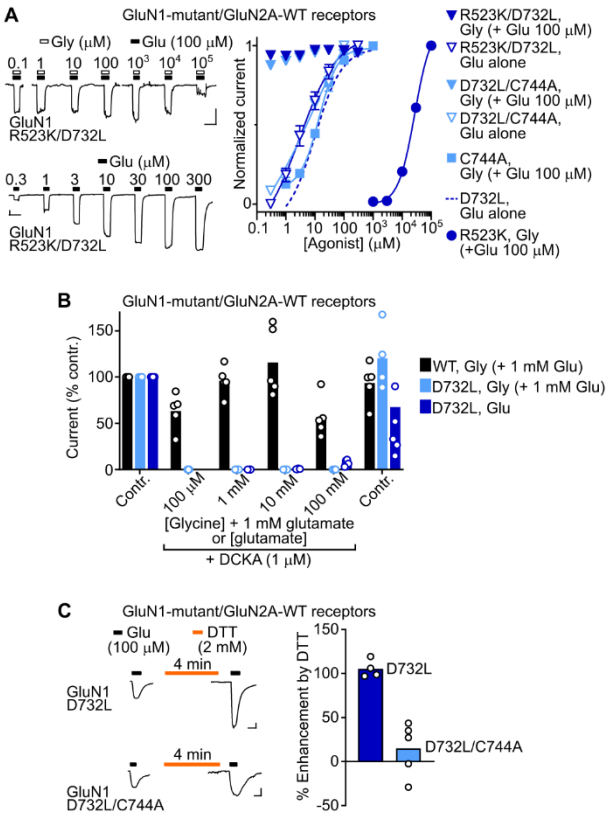

Figure 2. GluN1 D732L/F LBDs are constitutively active in the absence of ligands.

(**A**) *Left*, example ligand-gated currents in *Xenopus laevis* oocytes expressing NMDA receptors comprising GluN1-R523K/D732L and GluN2A-WT subunits. Scale bars: x, 10 s; y, 0.1 µA. *Right*, concentration-current response relationships (data points mean ± SEM, n = 3-5) for receptors carrying indicated GluN1 subunits together with WT GluN2A subunits.

(**B**) Mean (columns) and individual data points (n = 4-6) of glycine (+ 1 mM glutamate) -gated currents in GluN1-WT and GluN1-D732L-containing receptors and glutamate-gated currents in GluN1-D732L-containing receptors in the absence (control, "contr.") or presence of 1 µM 5,7-dichlorokynurenic acid (DCKA).

(**C**) *Left*, example ligand-gated currents, before and after dithiothreitol (DTT) treatment, in *Xenopus laevis* oocytes expressing NMDA receptors comprising indicated mutant GluN1 subunits and WT GluN2A subunits. Scale bars: x, 10 s; y, 0.5 µA. *Right*, mean (columns) and individual data points (n = 4-5) of % enhancement of current amplitude by DTT.

Seeking complementary evidence that glutamate does not bind to mutant GluN1 subunits, we measured competition for the GluN1 LBD between glutamate and 5,7-dichlorokynurenic acid (DCKA), a GluN1-selective competitive antagonist. Neither glutamate at concentrations up to 100 mM, nor glycine in the presence of glutamate were able to relieve DCKA-induced inhibition of GluN1-

D732L/GluN2A-WT receptors, in contrast to WT receptors, where even 100 µM glycine relieved more than 50% DCKA-induced inhibition (Fig. 2B). This shows that DCKA binding is intact in GluN1-D732 mutants and is further indicative that activation of GluN1-D732L/GluN2A WT-receptors by glutamate is not via glutamate binding to mutant GluN1 subunits.

Glycine and glutamate-gated currents through NMDA receptors are enhanced by the breaking of a native disulfide bond between cysteine residues C744, just four helical turns after D732, and C798, in the segment linking the LBD to membrane-spanning helix 4 ("LBD-M4", Fig. 1A, (27)). We questioned if this redox modulation is intact in GluN1-D732L/F-containing NMDA receptors given the proximity of the GluN1-732 position to C744. To this end, we tested the activity of double-mutant GluN1-D732L/C744A-containing receptors, in which the disulfide is not possible. GluN1-D732L/C744A-containing receptors were activated by glutamate alone (EC_{50} = 21 ± 4 µM, n = 4, Fig. 2A), indicating that constitutive activity of GluN1-D732L subunits does not rely on the C744-C798 disulfide. Moreover, DTT-induced enhancement of glutamate-gated currents was intact in single-mutant GluN1-D732L-containing receptors, and this was abolished by the addition of the C744A mutation (Fig. 2C). Thus, the hydrophobic plug in mutant receptors and glycine binding in WT receptors both induce an active GluN1 subunit that is enhanced by the reduction of the C744-C798 disulfide.

D732-αI interactions are replaced by Q536-αI interactions during GluN1 activation by glycine

Our results with mutant receptors suggest that the 732 side chain controls ligand potency and channel activity, and we therefore asked how D732 mediates these roles in WT channels. D732 movements during GluN1 activation can be inferred from previously published X-ray structures of the isolated GluN1 LBD in competitive antagonist-bound inactive, ligand-free inactive, and glycine-bound active states (Fig. 3A). The D732 side chain is positioned to accept hydrogen (H) bonds from A734 and V735 of the αI helix in inactive states, but swings centrally in the glycine-bound state to interact with the agonist amine (Fig. 3A). We reasoned that replacing A734 and V735 NH groups with an H bond acceptor would remove D732—αI interactions specific to inactive states and bias D732 toward its active position, resulting in either increased glycine potency or constitutive GluN1 activity similar to GluN1-D732L and D732F. We therefore measured activity of NMDA receptors in which GluN1 A734 and V735 were replaced by their α-hydroxy acid analogues, lactic acid (Aah) and 2-hydroxy-3-methylbutyric acid (Vah) via the nonsense suppression method (Fig. S1). However, neither the A734Aah nor the V735Vah substitution caused constitutive activity or an increase in glycine potency (Fig. 3B), indicating that the removal of single D732—αI interactions is not sufficient to bias the GluN1 subunit toward the active state.

The A734Aah substitution in fact caused a fourfold *decrease* in glycine potency (EC_{50} values 10.6 ± 0.6 µM, n = 6 for A734Aah and 2.4 ± 0.3 µM, n = 6, for

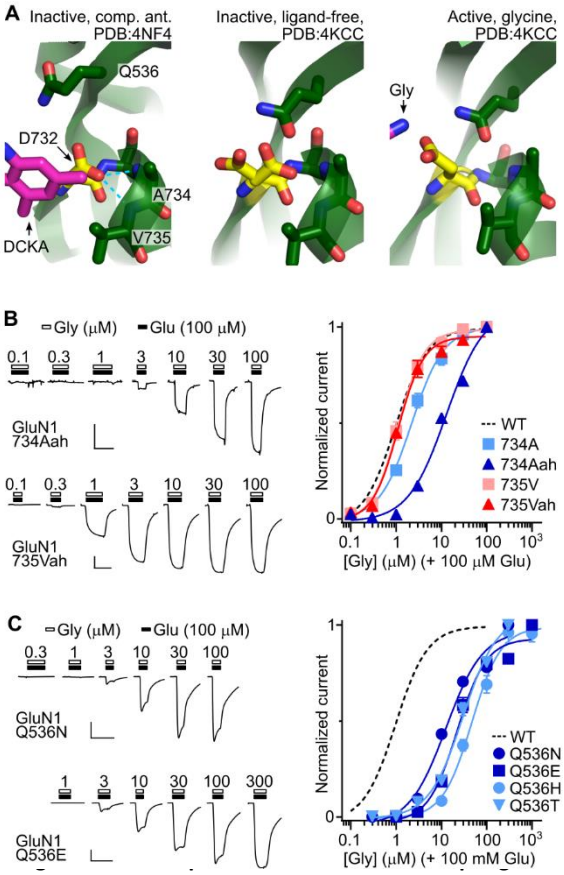

from A734 during LBD activation.
(**A**) D732 in indicated GluN1 X-ray structures. *Comp. ant.*, competitive antagonist, 5,7-dichlorokynurenic acid (DCKA). Dashed lines, putative H-bonds.
(**B,C**) *Left*, example ligand-gated currents in *Xenopus laevis* oocytes expressing NMDA receptors comprising indicated mutant GluN1 subunits and WT GluN2A subunits. *Aah*, lactic acid. *Vah*, 2-hydroxy-3-methylbutyric acid. *Right*, concentration-current response relationships (data points mean ± SEM, n = 5-7) for receptors carrying indicated GluN1 subunits together with WT GluN2A subunits.

WT in the nonsense suppression method; Fig. 3B, Fig. S1). We now considered that this decrease in potency may result from the loss of some interaction with the A734 NH that is conducive to the active state. We therefore re-examined the glycine-bound structure and observed that the GluN1 Q536 side chain from β-strand 12 in the LBD hinge region essentially moves 6 Å from the competitive antagonist-bound state and 0.4 Å from the ligand-free state toward both the A734 NH and the D732 COOH (Fig. 3A). Thus, the decreased glycine potency in GluN1-A734Aah may be via the loss of an A734 amine—Q536 amide bond that stabilizes the active LBD. We tested this interpretation by measuring the effects of conventional Q536N, -E, -T, and -H substitutions, which decrease the length of the amide side chain (Q536N), remove a hydrogen bond donor (Q536E), or replace the amide side chain with smaller or larger polar moieties (Q536T, Q536H). We observed 15-fold (Q536N, EC_{50} = 15 ± 0.6 μM, n = 5) to 50-fold (Q536H, EC_{50} = 51 ± 5 μM, n = 5) decreases in glycine potency in these mutants (Fig. 3C), indicating that the amide moiety and to a slightly smaller extent the length of the Q536 side chain are significant determinants of glycine-induced activation. Combined with existing X-ray structures, this suggests that D732 is important for glycine-induced activation of the WT LBD in part because glycine binding to one carboxylate oxygen of D732 exposes the αI-A734 amine to the Q536 amide oxygen. This conformation is in turn stabilized by the other D732 carboxylate oxygen interacting with the Q536 amide nitrogen, as implied by previous X-ray structural studies (13, 20).

A hydrophobic plug does not cause constitutive activity in all NMDA receptor subtypes

We next asked if D732 substitutions have a similar effect on NMDA receptor activity when the substitution is present in other subunits than GluN1 or when mutant GluN1 subunits are combined with other WT subunits than GluN2A. First, we measured the activity of receptors containing GluN1-WT and GluN2A-D731L or D731F subunits, as GluN2A-D731 aligns with GluN1-D732. GluN1-WT/GluN2A-D731L and -D731F receptors were not activated by glycine alone and were barely activated by high concentrations of glutamate in the presence of 100 μM glycine (Fig. 4A). We observed the same stark loss of function with the larger hydrophobic GluN2A-D731W substitution, and a less drastic but still >1000-fold decrease in glutamate potency with GluN2A-D731A/N/E substitutions (Fig.

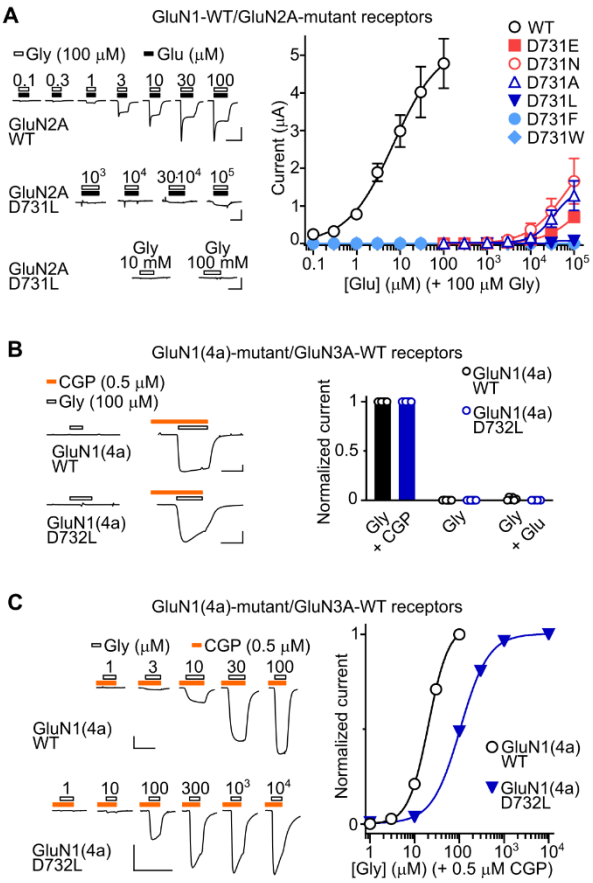

Figure 4. Effects of D732 substitutions in different NMDA receptor subtypes.
(**A**) *Left*, example ligand-gated currents in *Xenopus laevis* oocytes expressing NMDA receptors comprising WT GluN1 subunits and WT or mutant GluN2A subunits, as indicated. *Right*, concentration-current response relationships (data points mean ± SEM, n = 10 (WT), 3 (D731F and D731W), or 5-6 (all other mutants)) for receptors carrying WT GluN1 subunits together with indicated WT or mutant GluN2A subunits. (**B**) *Left*, example currents in oocytes expressing NMDA receptors comprising indicated WT or mutant GluN1 (4a isoform) subunits and WT GluN3A subunits in response to glycine alone or glycine in the presence of CGP 78608 (CGP). *Right*, mean (columns) and individual data points (n = 4-6) for current amplitude in the presence of different ligands (each 100 μM), normalized to current in the presence of glycine (100 μM) + CGP (0.5 μM). (**C**) *Left*, example currents in oocytes expressing NMDA receptors comprising indicated WT or mutant GluN1 (4a isoform) subunits and WT GluN3A subunits. *Right*, concentration-current response relationships (data points mean ± SEM, n = 6 (WT) or 5 (D732L)) for receptors carrying indicated GluN1 subunits.

4A). Thus, substitutions at the D732 (or equivalent) position decrease ligand potency in both GluN1 and GluN2A subunits, but leucine and phenylalanine substitutions induce constitutive LBD activation only in GluN1 subunits.

Second, we tested the effects of constitutive GluN1-D732L LBD activity in hetero-tetrameric GluN1/GluN3A NMDA receptors. GluN1/GluN3A receptors are glycine-gated channels that mediate relatively small currents in response to glycine, because despite glycine binding to and activating GluN3A subunits, glycine binding to GluN1 subunits deactivates the channel (28, 29). As GluN1/GluN3A receptors are assembled more efficiently by the GluN1(4a) isoform than the GluN1(1a) isoform (30) that we used above, we used GluN1(4a) for these experiments, after first confirming that the D732L substitution also generates solely glutamate-gated currents in GluN1(4a)-D732L/GluN2A-WT receptors (Fig. S2). Glycine alone activated no detectable currents in GluN1(4a)-D732L/GluN3A-WT receptors, and large glycine-gated currents were only observed in the presence of the GluN1-selective competitive antagonist CGP 78608, much like WT channels in our hands (Fig. 4B). We did observe, however, that the potency of glycine in activating GluN1(4a)/GluN3A receptors in the presence of CGP 78608 was decreased in GluN1(4a)-D732L-containing receptors, compared to WT (Fig 4C). Whether this derives from putative constitutive activity of GluN1(4a)-D732L inducing even greater channel deactivation than glycine binding to GluN1(4a)-WT, or from GluN1(4a)-D732L potentially having decreased CGP 78608 sensitivity, we did not explore.

Taken together, these experiments show that across NMDA receptor subtypes, D732L (or equivalent) substitutions generally decrease apparent ligand affinity in the mutated subunit but (a) only lead to constitutive LBD activation in certain subunits and (b) in the case of constitutive LBD activation have a different effect on channel activity depending on the type of hetero-tetramer.

Constitutive activity of a homomeric iGluR with a naturally occurring hydrophobic plug

The effects of a hydrophobic plug in the LBD thus differ among relatively complex NMDA receptors, in which the GluN1 subunits occupy the more accessory “A” and “C” positions in the hetero-tetramer (Fig. 1A, (12)). We questioned if iGluRs of simpler homo-tetrameric architecture might be more susceptible to channel activation by a hydrophobic plug. To answer this, we turned to the natural diversity of the iGluR superfamily and sought a wildtype receptor in which a naturally occurring substitution at the D732 (or equivalent) position might have been retained during evolution. We assembled diverse iGluR sequences, covering all animal lineages and animal iGluR families (Fig. 5A,B), and investigated variation at the D732 position. As expected, a carboxylate side chain at this position is highly conserved, with glutamate or aspartate occurring here in most members of each iGluR family (Fig. 5C). We identified one remarkable exception, however, with one gene from the AMPA-kainate-delta-phi family (AKDF, (5)) encoding a large hydrophobic tyrosine residue at this position (Fig. 5C). This iGluR gene, TRIADDRAFT_19383 from the placozoan *Trichoplax adhaerens* (henceforth $AKDF^{19383}$), is not found in other animal lineages, but it is conserved in two geographically distinct populations of *Trichoplax* and in a second placozoan species *Hoilungia hongkongensis* (Fig. S3A,B) (31-33). Moreover, the $AKDF^{19383}$ orthologue in each of the three animals has retained the tyrosine residue, despite divergence at other positions in the gene (Fig. S3A,B).

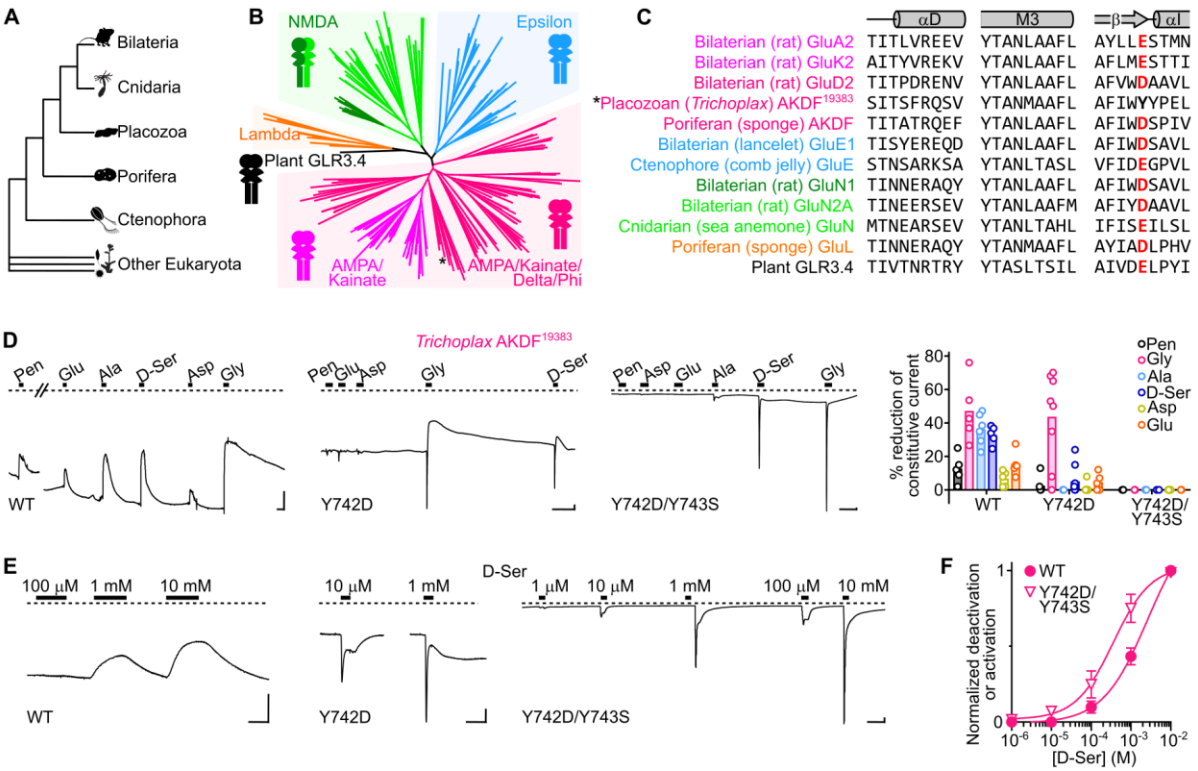

Figure 5. Constitutive activity of an iGluR with a naturally occurring hydrophobic plug.
(**A**) Overview of major animal lineages.
(**B**) Phylogeny of animal iGluR genes, rooted to plant iGluR 3.4 (black tip) as outgroup, colored and labelled by phylogenetic families. Cartoons indicate obligate heteromeric NMDA receptors and homomer-capable other receptors.
(**C**) Amino acid sequence alignment of selected ligand-binding domain segments (helix αD; helix αI with preceding β-strand) and membrane-spanning channel segment (M3) from characterized (except for poriferan lambda and AKDF) members of each iGluR family. Position equivalent to GluN1 D732 is highlighted red when conserved as a carboxylate side chain. Asterisk indicates *Trichoplax* AKDF^{19383} gene.
(**D**) Constitutive current (dashed line = zero current) and responses to different ligands in oocytes expressing indicated wildtype (WT) or mutant *Trichoplax* AKDF^{19383} receptors. Asp, L-aspartate. Glu, L-glutamate. D-Ser, D-Serine. Gly, glycine. Ala, alanine. Pent, pentamidine, an iGluR channel blocker.
(**E**) Current responses to increasing concentrations of D-serine in oocytes expressing indicated *Trichoplax* AKDF^{19383} receptors.
(**F**) Mean ± SEM (n = 4) deactivation normalized to maximum deactivation for WT and activation normalized to maximum activation for mutant Y742D/Y743S *Trichoplax* AKDF^{19383} receptors.

When we expressed *Trichoplax* AKDF^{19383} in *Xenopus* oocytes, we observed substantial current in the absence of ligands (390 ± 70 nA, n = 10 *cf.* 100 ± 20 nA, n = 8 in water-injected oocytes). The application of glycine, alanine, and D-serine but not glutamate or aspartate (each 10 mM) caused ~50% *inhibition* of this current (Fig. 5D), indicating that AKDF^{19383} receptors are constitutively active, and ligand binding induces channel deactivation. To test if the constitutive activity is mediated by the Y742 residue, we tested the activity of mutant Y742D AKDF^{19383} receptors. Remarkably, glycine and D-serine, and to a lesser extent glutamate, activated inward currents through Y742D receptors (Fig. 5D, mean glycine-gated current 1.8 ± 0.6 μA, n = 7). Ligand-gated currents were rapidly activating and deactivating in the continued presence of ligands (Fig. 5D), reflecting "desensitization" common to several iGluRs of the AKDF family, such as mammalian AMPA and kainate receptors (4). Constitutive currents were still present in mutant channels but in contrast to WT channels, these were not inhibited by the pore blocker pentamidine or by most agonists (Fig. 5D). The agonist glycine, however, induced desensitization that exceeded glycine-gated inward current amplitude, such that glycine effectively inhibited some of the constitutive current (Fig. 5D). Thus, a tyrosine or aspartate residue at the 742 position determines whether AKDF^{19383} is a constitutively active receptor inhibited by ligand-binding and conventional pore-blockers or is instead a principally ligand-gated channel that retains some constitutive activity.

We noticed that AKDF^{19383} has an additional tyrosine residue immediately following Y742, again differing from other iGluRs, which instead typically possess a small serine, glycine, or alanine at this position (Fig. 5C). We therefore generated and tested double-mutant Y742D/Y743S AKDF^{19383} receptors and now observed large ligand-gated currents and a total reduction of the constitutive current (Fig. 5D). Thus, amino acid residues at LBD positions 742 and 743 together account for channel activity of the *Trichoplax* AKDF^{19383} iGluR.

Finally, we measured ligand potency in WT and mutant *Trichoplax* AKDF^{19383}, to assess whether position 742 determines ligand potency in addition to channel activity. For these experiments we employed D-serine, as recovery from glycine-induced deactivation was very slow (Fig. 5D). Substantial deactivation of WT receptors was only induced by millimolar D-serine concentrations (Fig. 5E,F). In contrast, single- and double-mutants were activated by micromolar concentrations (Fig. 5E), with an EC_{50} of 490 ± 120 µM at Y742D/Y743S (n = 4; Y742D EC_{50} not assessed due to slow recovery from desensitization). Thus, a naturally occurring hydrophobic plug at the top of the β-strand preceding the αI helix leads to both constitutive activity and low ligand potency in a homo-tetrameric receptor from the AKDF iGluR family, and its removal via aspartate substitution reinstates ligand-gated currents and increases ligand potency. This is remarkably consistent with results in the GluN1 subunit of distantly related NMDA receptors, pointing toward a dominant role of this residue in LBD activation throughout the iGluR superfamily.

DISCUSSION

Seeking to understand which amino acid residues control iGluR activation and to facilitate the prediction of function from sequence, we investigated the role of a broadly conserved carboxylate residue in the middle of the iGluR LBD. Our experiments with heteromeric NMDA receptors and with a distantly related homomeric AKDF iGluR suggest that this residue controls agonist potency in most iGluRs and has a profound link to channel gating in certain iGluRs.

D732 in ligand-induced channel gating

That D732 should affect agonist potency in diverse iGluRs is not surprising. Previous reports show decreased agonist potency in NMDA receptors and AMPA receptors carrying mutations at the homologous aspartate and glutamate residue, respectively (21, 34), and X-ray structures of isolated GluN1, GluN2A, and GluA2 LBDs place the carboxylate ~3 Å from the amine of agonists glycine or glutamate (13, 14, 35). Our study suggests that D732 conformational change, and simply amino acid identity in unliganded receptors, controls channel activity, warranting further consideration of this residue in future studies dissecting the conformational changes that underlie iGluR activation.

Several ligand-induced conformational changes occur during ligand binding and before channel opening, as shown by kinetic descriptions of NMDA receptor single channel openings and closures (e.g. (36, 37)). Distinct pre-gating steps have also been identified in AMPA receptors via time-resolved fluorescence- and infrared-based analyses: a fast, preliminary “docking” of ligand to the upper lobe; and then a slower “locking” in which the lower lobe closes around the ligand (38, 39). And remarkably, E726 (≈ GluN1 D732) mutations primarily impair the slower, locking reaction (38, 39). If these pre-gating steps are similar in NMDA receptors, it is easy to imagine that glycine/glutamate binds to GluN1/GluN2 upper lobes during docking, and that the 732 side chain swings toward the ligand amine during locking. Consistent with this, cryo-electron microscopy of GluN1/GluN2B receptors captured two glycine- and glutamate-bound inactive conformations that likely precede channel opening, and the “less-active” of these shows D732 still oriented toward A734 and V735 of the αI helix, whereas in the second, D732 has swung toward glycine, although the ligand is not resolved in these 4 Å maps (12). If the D732 side chain is shorter, longer, and or non-carboxylate, docking presumably becomes less favourable, potentially explaining the large decrease in agonist potency at GluN1-D732A/S/N/E/Y/W and GluN2A-D731A/N/E/L/F/W mutants, and at WT AKDF^{19383} relative to Y742D AKDF^{19383} mutants.

Higher resolution X-ray structures of isolated NMDA receptor LBDs also capture the D732 carboxylate in two alternative conformations, swinging ~3 Å toward glycine during activation (Fig. 3A, (13, 20, 40)). Further analysis of these structures shows D732 movement is intricately coupled to Q536 side chain reorientation, which is supported by our experiments suggesting that interactions between Q536, from a β-sheet in the LBD hinge, and αI-A734 contribute to glycine potency in the GluN1 LBD. Thus, D732 could contribute to locking and further conformational changes by mediating coupling between (a) glycine binding and (b) hinge and αI conformation. Similar coupling was suggested for AMPA receptors, where ligand binding links the rearrangement of E726 during a late ligand-binding step to substantial lower lobe movement and even secondary structure changes, especially in the β-sheet below E726 in AMPA receptors (38, 41, 42). How this LBD movement is then transduced to channel opening is beyond our study, but as the LBD-M1, -M3, and -M4 linkers play distinct roles in later pre-gating steps (11, 12), perhaps future studies may link D732 rearrangement to distinct structural changes closer to the channel.

GluN1 and AKDF^{19383} receptors with a hydrophobic plug overcome most of these pre-gating and gating steps in the absence of ligand. Given the similarities between glycine and glutamate-gated WT NMDA receptors and solely glutamate-gated GluN1-D732L NMDA receptors, we think that similar LBD closure is induced by ligand binding and hydrophobic plugging. How the hydrophobic plug mediates this, we can only speculate, in the absence of structural data. Perhaps it re-positions water molecules linked to ligand-induced LBD closure (43), bridges the lower lobe directly to upper lobe hydrophobic side chains to close the LBD, and/or allows better access of β12-Q536 to αI-A734. Molecular dynamics simulations that map LBD energetics and correlate amino acid movements/interactions with LBD closure (20, 43) may offer the answer, especially if they can be extended to full-length structures of NMDA receptors (12, 22). We also envisage that structural studies of mutant GluN1-D732L/F NMDA receptors or WT AKDF^{19383} receptors might help capture subunits and/or receptors in distinct pre-gating or open states.

Physiological implications

iGluRs mediate most excitatory signals in the mammalian brain, and whereas AMPA receptors do the bulk of this work, NMDA receptors make vital contributions because of their distinct functional properties. These include high calcium ion permeability, the requirement for prior AMPA receptor activation, and via their obligate GluN1/GluN2 heteromeric nature the requirement for two different ligands. Our work shows that only small changes in the GluN1 LBD are required for solely glutamate-gated currents. Indeed, GluN1/GluN2 NMDA receptors from the arthropod *Drosophila melanogaster* and the mollusc *Aplysia californica*, in which D732 is conserved, are robustly activated by NMDA or aspartate in the absence of glycine (44, 45). Notably, glutamate-gated activation of these receptors still requires the co-agonist glycine (45), suggesting that glutamatergic synapses in both vertebrate and invertebrate bilaterian animals rely on a system of ambient glycine or D-serine (46, 47).

Genetic knock-in of solely glutamate-gated NDMA receptors via a single D732L/F mutation would allow the comparison of co-agonist-dependent and -independent NMDA receptors on other mutant backgrounds (e.g. phgdh$^{-/-}$ or SR$^{-/-}$ (47, 48)) to establish the precise contributions of co-agonists to NMDA receptor activity *in vivo*. Solely glutamate-gated and glycine-gated mutant rat NMDA receptors were reported previously after the introduction of pairs of cysteine residues in the upper and lower lobes of GluN1 or GluN2A subunits, respectively (23, 24). But as these rely on redox environment, which modulates WT NMDA receptors via native GluN1 disulfides (49), these cysteine-mutants are less suited to knock-in studies.

Biological implications

The dominant role of a broadly conserved residue on agonist potency and channel activity prompted us to ask if we could predict function from amino acid sequence. Predicting *ligand potency* based on amino acid identity at the 732 (or equivalent) position holds for GluN1, GluN2A, and GluN3 NMDA receptor subunits as well as *Trichoplax* AKDF^{19383} receptors, as an aspartate residue is conducive to higher potency and other residues to lower potency. But predicting *channel activity* – ligand-gated or

constitutively active – simply based on identity of this residue is more tenuous. In GluN1/GluN2A NMDA receptors, the induction of a constitutively active subunit by the L/F substitution is unique to GluN1 subunits. It is remarkable, however, that even in the distantly related homotetrameric AKDF^{19383} receptor, we see a similar pattern to GluN1, where an aspartate residue at this position is conducive to potently ligand-gated currents, and a large hydrophobic tyrosine side chain causes decreased ligand potency and constitutive channel activity. The pattern is not absolutely conserved, however, as only leucine and phenylalanine – not tyrosine – caused constitutive activity of GluN1 subunits.

The identification of a constitutively active iGluR channel from *Trichoplax* is striking. This adds iGluRs to the list of ligand-gated channel superfamilies in which leak channels have been identified, including for example degenerin/epithelial sodium channels and pentameric ligand-gated ion channels (50, 51). AKDF^{19383} orthologues are conserved in all three identified strains of placozoans, simple, flat animals with relatively few cell types (52). Single-cell RNA sequencing of *Trichoplax adhaerens* suggests that AKDF^{19383} is expressed in lipophil cells (53). These are large, unciliated columnar cells, interspersed between ventral epithelial cells and essentially bridging the ventral exterior with the interior of the animal (54). Classical neurons or synapses are probably absent from placozoans, as inferred from co-expression of typical pre- and post-synaptic proteins in *Trichoplax adhaerens* (33, 53), but previous reports of altered feeding in response to bath application of glycine and glutamate (55) and intercellular peptidergic signals from ventral ciliated cells (56) are indicative of chemosensory and integrative functions in these animals. Whether the AKDF^{19383} receptor behaves the same way in living placozoans as in our heterologous experiments is unknown, but we envisage it as a leak channel that is inhibited by small amino acid ligands either released from adjacent cells or found on the animal's substrate. Consideration of the equivalent residue in future sequencing projects will likely help distinguish constitutively active from typical, ligand-gated receptors of the iGluR superfamily.

METHODS

Plasmids and molecular biology

Rattus norvegicus GluN1 (1a isoform) and GluN2A (the regular, long isoform) inserts within the multiple cloning site (MCS) of pcDNA3.1 without poly(A) tails were a gift from Dr. David MacLean (University of Rochester Medical Center). *Rattus norvegicus* GluN1 (4a isoform) and GluN3A containing a C-terminal DYKDDDDK and within the MCS of pcDNA3.1 were purchased from Genscript (ORa13617 and Ora44363, respectively). The *Trichoplax adhaerens* AKDF^{19383} sequence was established by additional genome annotation of the Genbank TRIADDRAFT_19383 sequence (Fig. S3), codon-optimized in iCodon (57), and commercially synthesized and cloned into a modified pSP64-poly(A) vector (full sequence in Supplemental text).

Mutations were generated with partially overlapping primers and PCR with Phusion Hot Start II DNA Polymerase (ThermoFisher) according to published guidelines (58). Inserts were fully sequenced via Sanger sequencing.

Plasmids were linearized via restriction digest at sites downstream of the coding sequence (Rat GluN1/2/3) or downstream of the poly(A) segment (*Trichoplax* AKDF^{19383}) and purified via ethanol precipitation or DNA Clean & Concentrator-5 columns (Zymo Research). mRNA was transcribed for 2-2.5 h with mMESSAGE mMACHINE kits (ThermoFisher, T7 for pcDNA3, SP6 for pSP64-poly(A)) following supplier's protocols including DNAse treatment and purified with RNA Clean & Concentrator-5 (Zymo Research) or RNAeasy (Qiagen) kits.

Non-canonical amino acid chemistry

General

All reactions were carried out using commercial materials and reagents without further purification unless otherwise noted. All reactions were monitored by thin layer chromatography (TLC) on silica gel plates (Keiselgel 60 F254, Merck) and/or ultra-performance liquid chromatography (UPLC).

Visualization of the spots on TLC plates was achieved by UV light and by staining the TLC plates in potassium permanganate and charring with a heat gun, unless otherwise stated.

UPLC refers to a Waters Acquity UPLC HClass instrument with Acquity PDA detector, QDA mass detector and quaternary solvent system; PDA: 210-350 nm. Acidic methods were run using varying gradients of acetonitrile and water with 5% 2 vol% formic acid (99%) in water on the following columns: Acquity CSH C18 column (2.1 x 50 mm 1.7 µm) at 0.8 mL/min; Acquity CSH-Phenyl Hexyl (CSH PH) column (2.1 x 50 mm 1.7 µm) ; HSS T3 column (2.1 x 50 mm 1.8 µm) at 0.8 mL/min. Basic methods were run using varying gradients of acetonitrile and water with 5% 2 vol% ammonia (28%) in water on the following columns: XBridge BEH C18 column (2.5 µm 2.1 x 50 mm) at 0.8 mL/min; XBridge BEH C8 column (2.5 µm 2.1 x 50 mm) at 0.8 mL/min. Eluents A: water, B: acetonitrile, C: 2 vol % ammonia (28%) in water, D: 2 vol % formic acid (99%) in water.

Products characterized by ^{1}H NMR was recorded on a Bruker Advance III HD 400 MHz spectrometer. Chemical shifts are expressed in parts per million values (ppm) and are designated as s (singlet); br s (broad singlet); d (doublet); t (triplet); q (quartet); quint (quintet) or m (multiplet).

Chromatography was performed on a Biotage Isolera using silica (normal phase) (SiliCycle SiliaSep Premium 25 µm or Biotage SNAP Ultra HP-Sphere 25 µm) or C18 (reverse phase) (Biotage SNAP Ultra C18 HP Sphere 25 µm) pre-packed cartridges; or by flash-column chromatography using silica gel (Fluorochem silica gel 60A 40-63 µm).

General procedure A

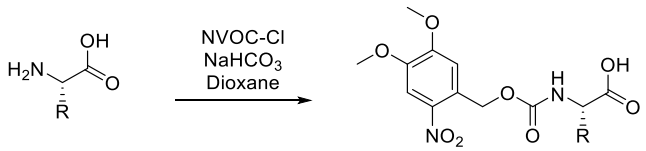

A suspension of amino acid (1 eq), (4,5-dimethoxy-2-nitro-phenyl)methyl carbonochloridate (1.1 eq) and sodium hydrogen carbonate (2.5 eq) in 1,4-dioxane (106 eq) was stirred at room temperature overnight. Water was added and stirred at room temp for 30 min. The reaction was diluted with ethyl acetate and the phases separated. The organic phase was discarded. The aqueous was acidified to ~pH 1 with 2 M HCl aqueous solution. The product was extracted with ethyl acetate and dried over $MgSO_4$. The solution was concentrated under vacuum to give the desired product which was used without purification in the next step.

General procedure B

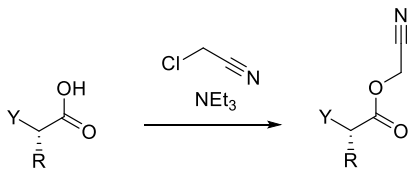

X = OH, NHNVOC

A stirring solution of NVOC-amino acid or 2-subsituted-2-hydroxyacetic acid (1 eq) and triethylamine (2 eq) in chloroacetonitrile (50 eq) was stirred at room temp overnight. The reaction mixture was concentrated under vacuum. The residue was suspended in EtOAc and sonicated for 10 min. The mixture was filtered and the filtrate concentrated under vacuum to give the desired cyanomethyl ester. Used in the next step without purification.

General procedure C

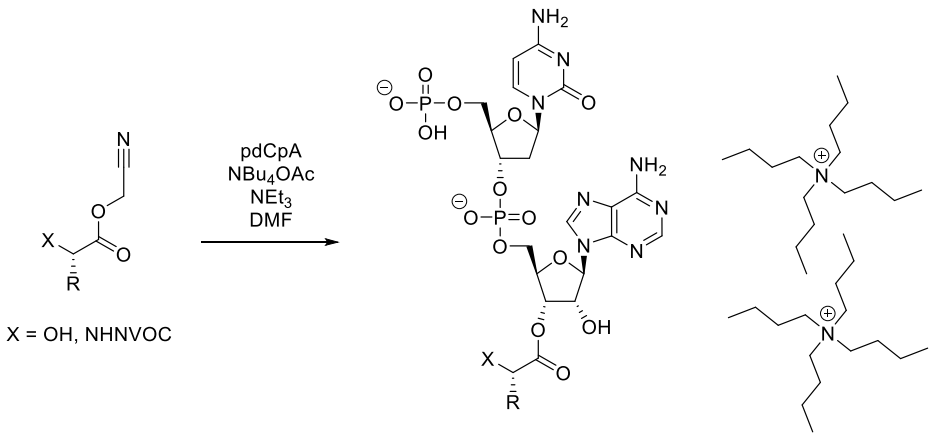

A solution of pdCpA (1 eq, synthesized according to (59)), cyanomethyl ester (1 eq), tetrabutylammonium acetate (2 eq) and triethylamine (2 eq) in *N*,*N*-dimethylformamide (70 eq) was stirred at 38 °C overnight. The reaction mixture was directly purified by reverse phase purification (Biotage Isolera, 12 g SiliaSep C18 cartridge; gradient 20-70% (acetonitrile + 0.1%formic acid) in (water + 0.1% formic acid) over 12 CV). The product containing fractions were freeze dried overnight to give the desired compound as a mixture of monoacylated isomers at the 3' and 2' positions.

Ditetrabutylammonium Nvoc-Val-OpdCpA

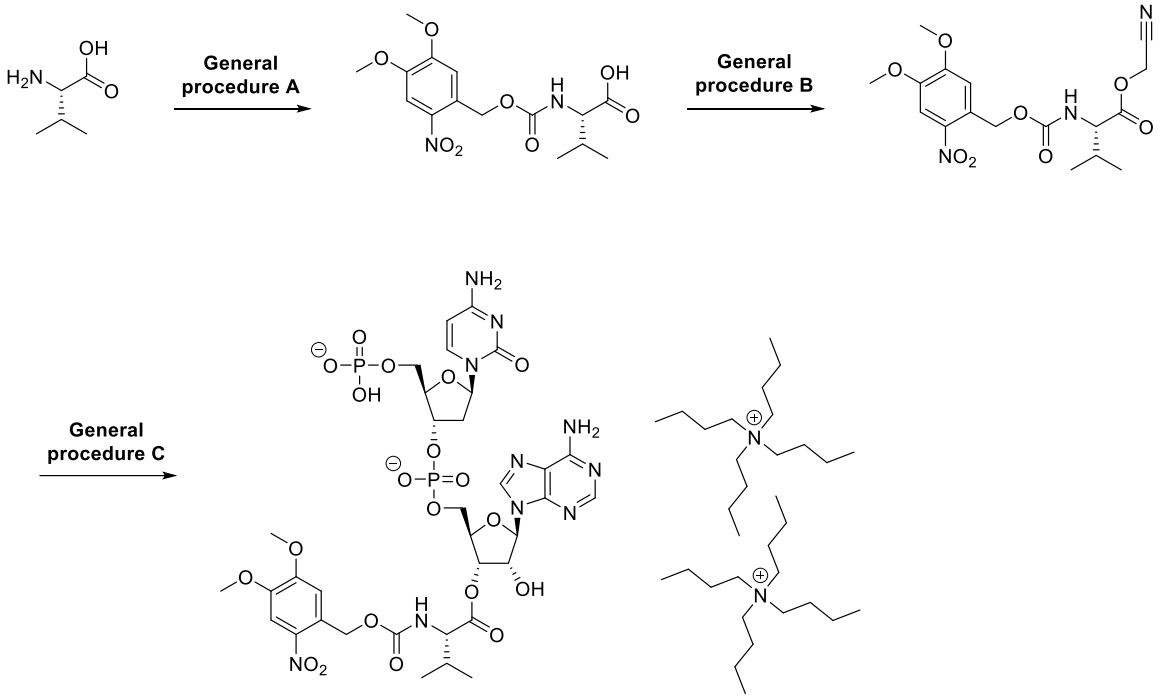

Using general procedure A, *L*-valine (58.0 mg, 1 eq, 0.495 mmol) gave the desired product Nvoc-Val-OH as yellow solid, 130 mg (74%). It was used in the next step without purification. UPLC-MS: (CSH-C18 Short Acid 2 to 95%, 1204-044-1) R_t = 0.79 min (83.7%), MS (ESIneg): m/z = $[M-H]^-$ 355.

Using general procedure B, Nvoc-Val-OH (119 mg, 1 eq, 0.334 mmol) gave the desired product Nvoc-Val-OCH_2CN as a yellow solid, 129 mg (98%). It was used in the next step without purification. UPLC-MS: (CSH-C18 Short base 2 to 95%, 1204-050-1) R_t = 0.86 min (90.7%), MS (ESIpos): m/z = $[M+Na]^+$ 418.

Using general procedure C, Nvoc-Val-OCH_2CN (12.0 mg, 1 eq, 31.4 µmol) gave the desired product, ditetrabutylammonium Nvoc-Val-OpdCpA as a white solid, 4.52 mg (9.3%).

UPLC-MS: (HSS T3 Long acid 0 to 10%, NBK2001-115-P1-2C) R_t = 1.78 min (30.2%), MS (ESIpos): m/z = $[M+H]^+$ 975; MS (ESIneg): m/z = $[M-H]^-$ 973 and 1.82 min (64.4%), MS (ESIpos): m/z = $[M+H]^+$ 975; MS (ESIneg): m/z = $[M-H]^-$ 973 – Combined purity of 94.6% (mixture of monoacylated isomers) (Fig. S4).

Ditetrabutylammonium Vah-OpdCpA

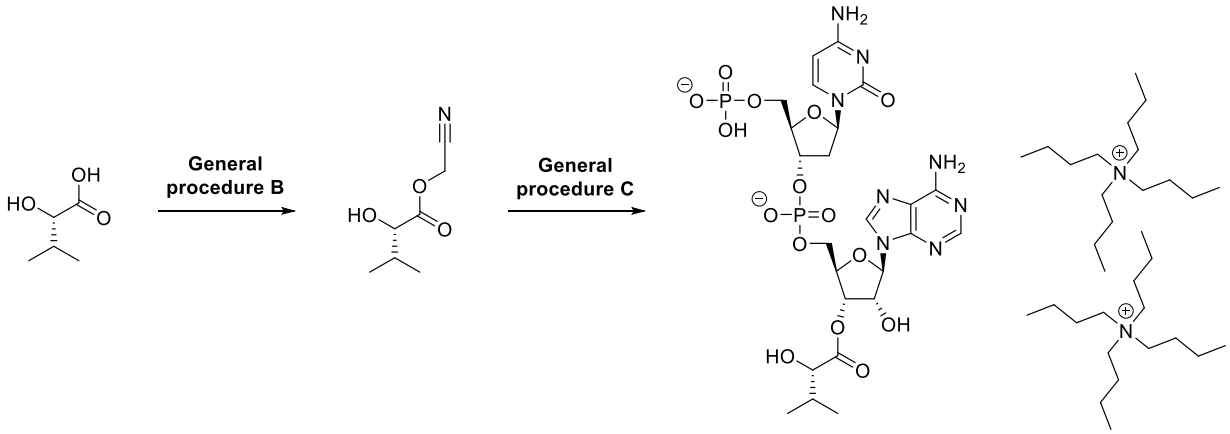

Using general procedure B, (*S*)-2-hydroxy-3-methylbutanoic acid (100 mg, 1 eq, 0.847 mmol) gave the desired product Vah-OCH_2CN as a colorless oil, 110 mg (83%). It was used in the next step without purification. ^{1}H NMR (400 MHz, $CDCl_3$, NBK2001-112-P1-1): δ [ppm] = 0.91 (d, 3H), 1.04 (d, 3H), 2.08-2.16 (m, 1H), 4.15 (d, 1H), 4.82 (q, 2H). 1 exchangeable proton not observed.

Using general procedure C, Vah-OCH_2CN (4.94 mg, 1 eq, 31.4 µmol) gave the desired product, ditetrabutylammonium Vah-OpdCpA as a white solid, 0.79 mg (2%).

UPLC-MS: (HSS T3 Long acid 0 to 10%, NBK2001-114-P1-2) R_t = 2.26 min (19.5%), MS (ESIpos): m/z = $[M+H]^+$ 737; MS (ESIneg): m/z = $[M-H]^-$ 735 and 2.60 min (80.1%), MS (ESIpos): m/z = $[M+H]^+$ 737; MS (ESIneg): m/z = [M-H]- 735 – Combined purity of 99.6% (mixture of monoacylated isomers). (Fig. S5.)

Ditetrabutylammonium Nvoc-Ala-OpdCpA

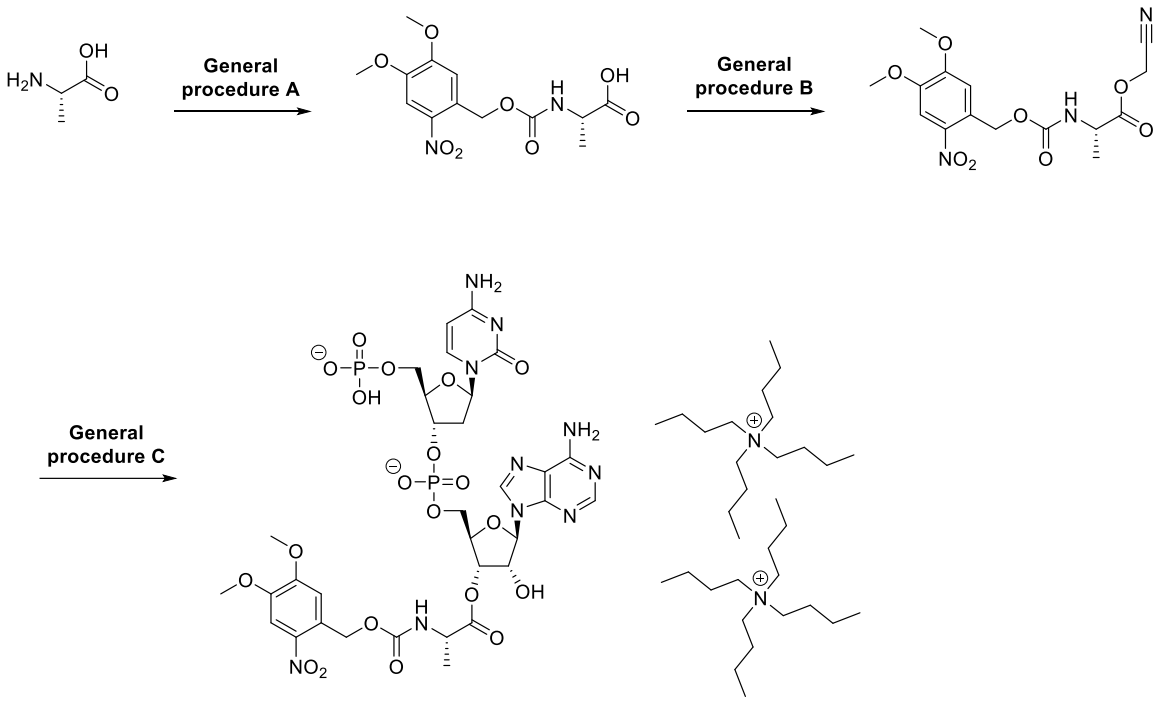

Using general procedure A, *L*-alanine (44.1 mg, 1 eq, 0.495 mmol) gave the desired product Nvoc-Ala-OH as yellow solid, 119 mg (73%). It was used in the next step without purification. UPLC-MS: (CSH-

C18 Short Acid 2 to 95%, 1204-045-1) R_t = 0.68 min (84.1%), MS (ESIpos): m/z = $[M+Na]^+$ 351; MS (ESIneg): m/z = $[M-H]^-$ 327.

Using general procedure B, Nvoc-Ala-OH (119 mg, 1 eq, 0.362 mmol) gave the desired product Nvoc-Ala-OCH_2CN as a yellow solid, 128 mg (96%). It was used in the next step without purification. UPLC-MS: (CSH-C18 Short Acid 2 to 95%, 1204-051-1) R_t = 0.75 min (78.8%), MS (ESIpos): m/z = $[M+Na]^+$ 390.

Using general procedure C, Nvoc-Ala-OCH_2CN (30.0 mg, 1 eq, 47.1 µmol) gave the desired product, ditetrabutylammonium Nvoc-Ala-OpdCpA as a white solid, 17.0 mg (38%).

UPLC-MS: (HSS T3 Long acid 0 to 20%, 1273-062-2) R_t = 2.85 min (46.6% at 254 nm), MS (ESIpos): m/z = $[M+H]^+$ 947; MS (ESIneg): m/z = $[M-H]^-$ 945 and 3.03 min (48.8% at 254 nm), MS (ESIpos): m/z = $[M+H]^+$ 947; MS (ESIneg): m/z = $[M-H]^-$ 945 – Combined purity of 95.4% (mixture of monoacylated isomers). (Fig. S6.)

Ditetrabutylammonium Aah-OpdCpA

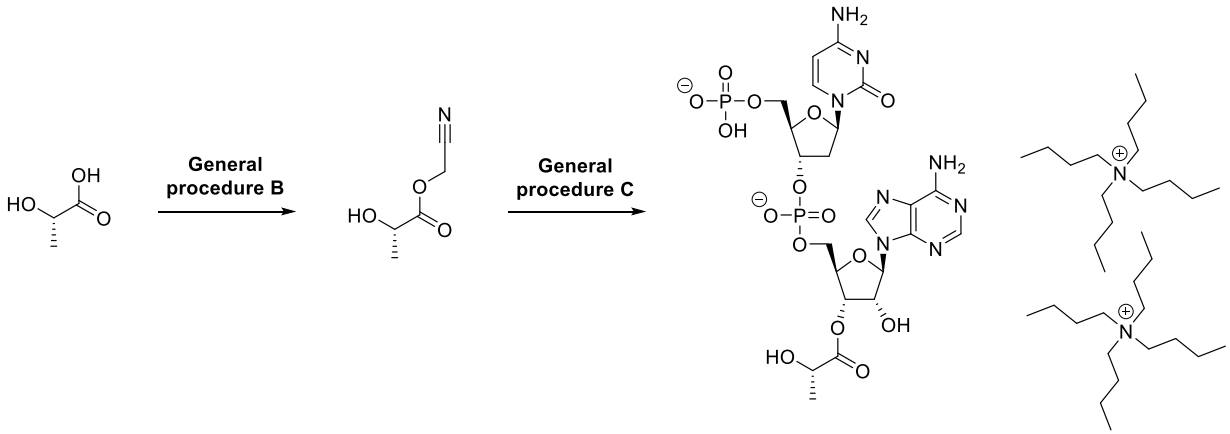

Using general procedure B, (*S*)-2-hydroxypropanoic acid (100 mg, 1 eq, 1.11 mmol) gave the desired product Aah-OCH_2CN, 95.0 mg (66%) as a colorless oil. It was used in the next step without purification. ^1H NMR (400 MHz, $CDCl_3$, NBK2001-111-P1-1): δ [ppm] = 1.47 (d, 3H), 4.41 (q, 1H), 4.81 (s, 2H). 1 exchangeable proton not observed.

Using general procedure C, Aah-OCH_2CN (4.06 mg, 1 eq, 31.4 µmol) gave the desired product, ditetrabutylammonium Aah-OpdCpA was isolated as a white solid, 2.60 mg (6.4%).

UPLC-MS: (HSS T3 Long acid 0 to 10%, NBK2001-113-P1-2) Rt = 1.55 min (22.3%), MS (ESIneg): m/z = $[M-H]^-$ 707 and 1.75 min (69.9%), MS (ESIpos): m/z = $[M+H]^+$ 709; MS (ESIneg): m/z = $[M-H]^-$ 707 – Combined purity of 92.2% (mixture of monoacylatedisomers). (Fig. S7.)

Channel expression and non-canonical amino acid incorporation

Defoliculated Stage V/VI *Xenopus laevis* frog eggs were purchased weekly from EcoCyte Bioscience and stored at 18 °C in 50% (in water) Leibovitz's L-15 medium (Gibco) supplemented with additional 0.25 mg/ml gentamicin, 1 mM L-glutamine, and 15 mM HEPES, pH 7.6.

For the expression of wildtype and conventional mutant channels, oocytes were injected with 2 ng (rat NDMA receptors) or 10 ng (*Trichoplax* AKDF[19383]) RNA in 40 nl water using a Nanoliter2010 injector and glass micropipettes (World Precision Instruments). Non-canonical amino acid mutant NMDA receptor channels were expressed by co-injecting oocytes with amber stop codon mutant GluN1(1a) mRNA, wildtype GluN2A mRNA, and aminoacylated tRNA (60). Modified *Tetrahymena thermophila* $tRNA^{Gln}$ (61) was prepared by ligation of forward and reverse DNA strands containing the T7 promotor (Merck), transcription of RNA with the T7-Scribe transcription kit (Cellscript), and purification in Chroma Spin DEPC-H20 columns (Clontech). This tRNA was ligated to Nvoc-Val-OpdCpA, Nvoc-Ala-OpdCpA, Vah-OpdCpA, and Aah-OpdCpA with T4 DNA ligase (New England Biolabs), and the product was purified

with phenol-chloroform extraction and ethanol precipitation and stored at −80°C until use. Immediately before injection into oocytes, precipitate was resuspended in 1 µl water, deprotected via UV light (Nvoc-Val-OpdCpA and Nvoc-Ala-OpdCpA only) in a coil of 365 nm realUV LED strip lights (Waveform Lighting) cooled with a fan, and mixed 2:1:1 with 800 ng/µl amber stop codon mutant GluN1 mRNA and 200 ng/µl wildtype GluN2A mRNA (Fig. S1). 40 nl of this mix was then injected into oocytes. Injected oocytes were stored in the same diluted L-15 medium (above) until electrophysiological recordings.

Two-electrode voltage clamp and data analysis

One to two days (rat NMDA receptors) or three to four days (*Trichoplax* AKDF^{19383}) after injection, each oocyte was placed in an RC-3Z bath (Warner Instruments) and continuously perfused with a bath solution of NaCl 100 mM, KCl 2.5 mM, BaCl2 0.3 mM, HEPES 5 mM, diethylenetriamine-pentaacetic acid 0.01 mM, pH 7.3 (rat NMDA receptors, to avoid inhibition by magnesium and zinc ions (62)) or NaCl 96 mM, KCl 2 mM, CaCl2 1.8 mM, MgCl2 1 mM, HEPES 5 mM, pH 7.5 (*Trichoplax* AKDF^{19383}). Bath solution was exchanged for that containing ligand as indicated in main text with a VCS-8-pinch valve control perfusion system (Warner Instruments). Ligands were stored as 1 M stocks in water (glycine) or 10 – 300 mM stocks in water or bath solution pH adjusted with NaOH (CGP 78608, monosodium glutamate, DCKA) and dissolved in bath solution before use. CGP 78608 was purchased from Tocris, all others from Merck. Oocytes were impaled with silver-chloride microelectrodes in 3M KCl-filled borosilicate micropipettes and clamped at −60 mV (rat NMDA receptors) or −80 mV (*Trichoplax* AKDF^{19383}) with an Oocyte Clamp OC-725D amplifier (Warner Instruments), Axon Digidata 1550B digitizer (Molecular Devices), and current was sampled at 500 or 1000 Hz and low-pass filtered at 100 or 200 Hz. Current amplitudes were measured in Clampfit 11.1 (Molecular Devices) including additional offline 20 Hz filtering (Bessel 8-pole) for display in figures.

Subsequent data analyses were performed in Prism v9 (GraphPad Software). For concentration-response data, peak current amplitude or peak decrease in current amplitude was plotted against ligand concentration and fitted with four parameter non-linear regression for each recording. These were averaged to give means ± SEM in main text, and a single fit to the average normalized responses (±SEM) is shown in figures.

Bioinformatic analyses

In generating a phylogenetic tree covering the broad superfamily of iGluRs in animals, we first assembled iGluR subunit amino acid sequences by blasting with NMDA receptor (rat GluN1) and AMPA receptor (rat GluA2) against two ctenophores (*Euplokamis dunlapae*, *Mnemiopsis leidyi*), one poriferan (*Oscarella carmela*), two cnidarians (*Aurelia aurita* - Roscoff strain, *Nematostella vectensis*), one placozoan (*Trichoplax adhaerens* – Grell strain), and from bilaterians two xenacoelomorphs (*Hofstenia miamia*, *Xenoturbella bocki*), two protostomes (*Crassostrea gigas*, *Lingula anatina*), three invertebrate dueterostomes (*Acanthaster planci*, *Saccoglossus kowalevskii*, *Branchiostoma belcheri*) and one vertebrate deuterostome (*Rattus norvegicus*) using published xenacoelomorph transcriptomes (63), the OIST Marine Genomics Unit database (*Aurelia aurita*, *Lingula anatina*), Joint Genome Institute (*Nematostella vectensis*), ENSEMBL Metazoa (*Mnemiopsis leidyi*) and NCBI (all others, except rat: from UniProt). Retrieved amino acid sequences lacking ligand-binding domain or channel-forming helices were excluded, duplicates of over 85% identity were excluded, and 212 remaining sequences were aligned in MAFFT (64) along with *Arabidopsis thaliana* (plant) GLR 3.4 as an outgroup (65), and this alignment was used to generate a GLR 3.4-rooted phylogeny with FastTree (66). The alignment and phylogeny can be freely downloaded from lynaghlab.com/resources. MAFFT and FastTree were used as plugins within Geneious Prime 2023 (Dotmatics). Secondary structure and relative position of amino acids in alignment extraction (Fig. 5C) are based on published NMDA receptor and AMPA receptor X-ray structures(22, 67).

The analysis of placozoan genes in Fig. S3 and Supplemental text utilized the *Trichoplax adhaerens* ("Grell") genome (33) and the *Trichoplax* sp. H2 ("Panama") genome (32), both retrieved from NCBI,

and the *Hoilungia hongkongensis* genome (31) retrieved from https://bitbucket.org/molpalmuc/hoilungia-genome/src/master/.

ACKNOWLEDGEMENTS

This project has received funding from the European Research Council (ERC) under the European Union's Horizon 2020 research and innovation programme (grant agreement no. 803714) and from The Research Council of Norway (project no. 234817). The authors are grateful to Adriana Alvizu (Michael Sars Centre) for help with molecular biology.

AUTHOR CONTRIBUTIONS

Conceptualization, SS, TL; Methodology, SS, OS, YW, HYH, TL; Investigation, SS, OS, YW, HYH; Resources, HYH; Writing – original draft, HYH, TL; Writing – review & editing, SS, OS, YW, HYH, TL; Visualization, OS, TL; Funding acquisition, TL.

DECLARATION OF INTERESTS

The authors declare no competing interests.

REFERENCES

1. L. G. Brock, J. S. Coombs, J. C. Eccles, The recording of potentials from motoneurones with an intracellular electrode. *The Journal of Physiology* **117**, 431-460 (1952).
2. T. G. Smart, P. Paoletti, Synaptic neurotransmitter-gated receptors. *Cold Spring Harb Perspect Biol* **4** (2012).
3. J. DeFelipe, L. Alonso-Nanclares, J. I. Arellano, Microstructure of the neocortex: Comparative aspects. *Journal of Neurocytology* **31**, 299-316 (2002).
4. K. B. Hansen *et al.*, Structure, Function, and Pharmacology of Glutamate Receptor Ion Channels. *Pharmacol Rev* **73**, 298-487 (2021).
5. D. Ramos-Vicente *et al.*, Metazoan evolution of glutamate receptors reveals unreported phylogenetic groups and divergent lineage-specific events. *Elife* **7** (2018).
6. R. Alberstein, R. Grey, A. Zimmet, D. K. Simmons, M. L. Mayer, Glycine activated ion channel subunits encoded by ctenophore glutamate receptor genes. *Proc Natl Acad Sci U S A* **112**, E6048-6057 (2015).
7. G. Q. Chen, C. Cui, M. L. Mayer, E. Gouaux, Functional characterization of a potassium-selective prokaryotic glutamate receptor. *Nature* **402**, 817-821 (1999).
8. I. H. Greger, J. F. Watson, S. G. Cull-Candy, Structural and Functional Architecture of AMPA-Type Glutamate Receptors and Their Auxiliary Proteins. *Neuron* **94**, 713-730 (2017).
9. K. B. Hansen *et al.*, Structure, function, and allosteric modulation of NMDA receptors. *J Gen Physiol* **150**, 1081-1105 (2018).
10. C. Luscher, R. C. Malenka, NMDA receptor-dependent long-term potentiation and long-term depression (LTP/LTD). *Cold Spring Harb Perspect Biol* **4** (2012).
11. J. B. Amin, A. Gochman, M. He, N. Certain, L. P. Wollmuth, NMDA Receptors Require Multiple Pre-opening Gating Steps for Efficient Synaptic Activity. *Neuron* **109**, 488-501 e484 (2021).
12. T. H. Chou, N. Tajima, A. Romero-Hernandez, H. Furukawa, Structural Basis of Functional Transitions in Mammalian NMDA Receptors. *Cell* **182**, 357-371 e313 (2020).
13. H. Furukawa, E. Gouaux, Mechanisms of activation, inhibition and specificity: crystal structures of the NMDA receptor NR1 ligand-binding core. *EMBO J* **22**, 2873-2885 (2003).
14. N. Armstrong, E. Gouaux, Mechanisms for activation and antagonism of an AMPA-sensitive glutamate receptor: crystal structures of the GluR2 ligand binding core. *Neuron* **28**, 165-181 (2000).
15. J. D. Clements, G. L. Westbrook, Activation kinetics reveal the number of glutamate and glycine binding sites on the N-methyl-D-aspartate receptor. *Neuron* **7**, 605-613 (1991).

16. T. C. Smith, J. R. Howe, Concentration-dependent substate behavior of native AMPA receptors. *Nat Neurosci* **3**, 992-997 (2000).
17. M. V. Yelshanskaya, D. S. Patel, C. M. Kottke, M. G. Kurnikova, A. I. Sobolevsky, Opening of glutamate receptor channel to subconductance levels. *Nature* **605**, 172-178 (2022).
18. A. C. Chin, R. A. Yovanno, T. J. Wied, A. Gershman, A. Y. Lau, D-Serine Potently Drives Ligand-Binding Domain Closure in the Ionotropic Glutamate Receptor GluD2. *Structure* **28**, 1168-1178 e1162 (2020).
19. A. Inanobe, H. Furukawa, E. Gouaux, Mechanism of partial agonist action at the NR1 subunit of NMDA receptors. *Neuron* **47**, 71-84 (2005).
20. Y. Yao, C. B. Harrison, P. L. Freddolino, K. Schulten, M. L. Mayer, Molecular mechanism of ligand recognition by NR3 subtype glutamate receptors. *EMBO J* **27**, 2158-2170 (2008).
21. K. Williams, J. Chao, K. Kashiwagi, T. Masuko, K. Igarashi, Activation of N-methyl-D-aspartate receptors by glycine: role of an aspartate residue in the M3-M4 loop of the NR1 subunit. *Molecular Pharmacology* **50**, 701 (1996).
22. E. Karakas, H. Furukawa, Crystal structure of a heterotetrameric NMDA receptor ion channel. *Science* **344**, 992-997 (2014).
23. M. L. Blanke, A. M. VanDongen, Constitutive activation of the N-methyl-D-aspartate receptor via cleft-spanning disulfide bonds. *J Biol Chem* **283**, 21519-21529 (2008).
24. C. L. Kussius, G. K. Popescu, NMDA receptors with locked glutamate-binding clefts open with high efficacy. *J Neurosci* **30**, 12474-12479 (2010).
25. A. Kuryatov, B. Laube, H. Betz, J. Kuhse, Mutational analysis of the glycine-binding site of the NMDA receptor: structural similarity with bacterial amino acid-binding proteins. *Neuron* **12**, 1291-1300 (1994).
26. B. Laube, H. Hirai, M. Sturgess, H. Betz, J. Kuhse, Molecular determinants of agonist discrimination by NMDA receptor subunits: analysis of the glutamate binding site on the NR2B subunit. *Neuron* **18**, 493-503 (1997).
27. J. M. Sullivan *et al.*, Identification of two cysteine residues that are required for redox modulation of the NMDA subtype of glutamate receptor. *Neuron* **13**, 929-936 (1994).
28. J. E. Chatterton *et al.*, Excitatory glycine receptors containing the NR3 family of NMDA receptor subunits. *Nature* **415**, 793-798 (2002).
29. C. Madry *et al.*, Principal role of NR3 subunits in NR1/NR3 excitatory glycine receptor function. *Biochem Biophys Res Commun* **354**, 102-108 (2007).
30. C. T. Smothers, J. J. Woodward, Expression of glycine-activated diheteromeric NR1/NR3 receptors in human embryonic kidney 293 cells Is NR1 splice variant-dependent. *J Pharmacol Exp Ther* **331**, 975-984 (2009).
31. M. Eitel *et al.*, Comparative genomics and the nature of placozoan species. *PLoS Biol* **16**, e2005359 (2018).
32. K. Kamm, H. J. Osigus, P. F. Stadler, R. DeSalle, B. Schierwater, Trichoplax genomes reveal profound admixture and suggest stable wild populations without bisexual reproduction. *Sci Rep* **8**, 11168 (2018).
33. M. Srivastava *et al.*, The Trichoplax genome and the nature of placozoans. *Nature* **454**, 955-960 (2008).
34. I. Mano, Y. Lamed, V. I. Teichberg, A venus flytrap mechanism for activation and desensitization of alpha-amino-3-hydroxy-5-methyl-4-isoxazole propionic acid receptors. *J Biol Chem* **271**, 15299-15302 (1996).
35. H. Furukawa, S. K. Singh, R. Mancusso, E. Gouaux, Subunit arrangement and function in NMDA receptors. *Nature* **438**, 185-192 (2005).
36. K. A. Cummings, G. K. Popescu, Glycine-dependent activation of NMDA receptors. *J Gen Physiol* **145**, 513-527 (2015).
37. A. J. Gibb *et al.*, A structurally derived model of subunit-dependent NMDA receptor function. *J Physiol* **596**, 4057-4089 (2018).

38. R. Abele, K. Keinanen, D. R. Madden, Agonist-induced isomerization in a glutamate receptor ligand-binding domain. A kinetic and mutagenetic analysis. *J Biol Chem* **275**, 21355-21363 (2000).
39. Q. Cheng, M. Du, G. Ramanoudjame, V. Jayaraman, Evolution of glutamate interactions during binding to a glutamate receptor. *Nat Chem Biol* **1**, 329-332 (2005).
40. A. Jespersen, N. Tajima, G. Fernandez-Cuervo, E. C. Garnier-Amblard, H. Furukawa, Structural insights into competitive antagonism in NMDA receptors. *Neuron* **81**, 366-378 (2014).
41. N. Armstrong, M. Mayer, E. Gouaux, Tuning activation of the AMPA-sensitive GluR2 ion channel by genetic adjustment of agonist-induced conformational changes. *Proc Natl Acad Sci U S A* **100**, 5736-5741 (2003).
42. R. L. McFeeters, R. E. Oswald, Structural mobility of the extracellular ligand-binding core of an ionotropic glutamate receptor. Analysis of NMR relaxation dynamics. *Biochemistry* **41**, 10472-10481 (2002).
43. S. L. Kaye, M. S. Sansom, P. C. Biggin, Molecular dynamics simulations of the ligand-binding domain of an N-methyl-D-aspartate receptor. *J Biol Chem* **281**, 12736-12742 (2006).
44. S. L. Carlson, A. T. Kempsell, L. A. Fieber, Pharmacological evidence that D-aspartate activates a current distinct from ionotropic glutamate receptor currents in Aplysia californica. *Brain Behav* **2**, 391-401 (2012).
45. S. Xia *et al.*, NMDA receptors mediate olfactory learning and memory in Drosophila. *Curr Biol* **15**, 603-615 (2005).
46. R. Bergeron, T. M. Meyer, J. T. Coyle, R. W. Greene, Modulation of N-methyl-D-aspartate receptor function by glycine transport. *Proc Natl Acad Sci U S A* **95**, 15730-15734 (1998).
47. S. Neame *et al.*, The NMDA receptor activation by d-serine and glycine is controlled by an astrocytic Phgdh-dependent serine shuttle. *Proc Natl Acad Sci U S A* **116**, 20736-20742 (2019).
48. J. H. Yang *et al.*, Brain-specific Phgdh deletion reveals a pivotal role for L-serine biosynthesis in controlling the level of D-serine, an N-methyl-D-aspartate receptor co-agonist, in adult brain. *J Biol Chem* **285**, 41380-41390 (2010).
49. G. Kohr, S. Eckardt, H. Luddens, H. Monyer, P. H. Seeburg, NMDA receptor channels: subunit-specific potentiation by reducing agents. *Neuron* **12**, 1031-1040 (1994).
50. C. M. Canessa *et al.*, Amiloride-sensitive epithelial Na+ channel is made of three homologous subunits. *Nature* **367**, 463-467 (1994).
51. K. Schnizler *et al.*, A novel chloride channel in Drosophila melanogaster is inhibited by protons. *J Biol Chem* **280**, 16254-16262 (2005).
52. B. Schierwater, R. DeSalle, Placozoa. *Current Biology* **28**, R97-R98 (2018).
53. A. Sebe-Pedros *et al.*, Early metazoan cell type diversity and the evolution of multicellular gene regulation. *Nat Ecol Evol* **2**, 1176-1188 (2018).
54. C. L. Smith *et al.*, Novel cell types, neurosecretory cells, and body plan of the early-diverging metazoan Trichoplax adhaerens. *Curr Biol* **24**, 1565-1572 (2014).
55. M. A. Nikitin, D. Y. Romanova, S. I. Borman, L. L. Moroz, Amino acids integrate behaviors in nerveless placozoans. *Front Neurosci* **17**, 1125624 (2023).
56. A. Senatore, T. S. Reese, C. L. Smith, Neuropeptidergic integration of behavior in Trichoplax adhaerens, an animal without synapses. *Journal of Experimental Biology* **220**, 3381-3390 (2017).
57. M. Diez *et al.*, iCodon customizes gene expression based on the codon composition. *Scientific Reports* **12**, 12126 (2022).
58. Y. Xia, W. Chu, Q. Qi, L. Xun, New insights into the QuikChange process guide the use of Phusion DNA polymerase for site-directed mutagenesis. *Nucleic Acids Res* **43**, e12 (2015).
59. X.-F. Zhu, A. I. Scott, An improved synthesis of the dinucleotides pdCpA and pdCpdA. *Nucleosides, Nucleotides & Nucleic Acids* **20**, 197-211 (2001).

60. D. A. Dougherty, E. B. Van Arnam, In vivo incorporation of non-canonical amino acids by using the chemical aminoacylation strategy: a broadly applicable mechanistic tool. *Chembiochem* **15**, 1710-1720 (2014).
61. M. E. Saks *et al.*, An engineered Tetrahymena tRNAGln for in vivo incorporation of unnatural amino acids into proteins by nonsense suppression. *J Biol Chem* **271**, 23169-23175 (1996).
62. P. Paoletti, P. Ascher, J. Neyton, High-affinity zinc inhibition of NMDA NR1-NR2A receptors. *J Neurosci* **17**, 5711-5725 (1997).
63. C. Andrikou, D. Thiel, J. A. Ruiz-Santiesteban, A. Hejnol, Active mode of excretion across digestive tissues predates the origin of excretory organs. *PLoS Biol* **17**, e3000408 (2019).
64. K. Katoh, K. Misawa, K. Kuma, T. Miyata, MAFFT: a novel method for rapid multiple sequence alignment based on fast Fourier transform. *Nucleic Acids Res* **30**, 3059-3066 (2002).
65. E. D. Vincill, A. M. Bieck, E. P. Spalding, Ca(2+) conduction by an amino acid-gated ion channel related to glutamate receptors. *Plant Physiol* **159**, 40-46 (2012).
66. M. N. Price, P. S. Dehal, A. P. Arkin, FastTree 2--approximately maximum-likelihood trees for large alignments. *PLoS One* **5**, e9490 (2010).
67. A. I. Sobolevsky, M. P. Rosconi, E. Gouaux, X-ray structure, symmetry and mechanism of an AMPA-subtype glutamate receptor. *Nature* **462**, 745-756 (2009).